High-Energy Detector Backgrounds from a Plasma Lens*

P. Chen, C.-K. Ng
Stanford Linear Accelerator Center
Stanford University, Stanford, CA 94309

and

A. W. Weidemann†
University of Tennessee, Knoxville, TN 37996

Abstract

Although proof-of-principle experiments have verified the self-focusing effect of a plasma lens, its utility as a linear-collider final-focusing element depends largely on the potential backgrounds that may be induced by the insertion of such a device at the interaction region of the detector. In this paper we identify different sources of such backgrounds, calculate their event rates from the elementary interaction processes, and evaluate their effects on the major parts of a hypothetical Next Linear Collider (NLC) detector. Using the proposed NLC design as a reference, we find that the background yields are small so that the performance of the main components of the detector will not be affected.

Submitted to Nuclear Instruments and Methods A

*Work supported by Department of Energy contracts DE–AC03–76SF00515 (SLAC) and DE–FG05–91ER40627 (Tennessee).

†Mailing Address: SLAC, MS 94, P.O.B. 4349, Stanford, CA 94309

1 Introduction

The use of a plasma lens as a final-focusing device to increase the luminosity in e^+e^- linear colliders was proposed some time ago [1]. Conventional quadrupole magnets for final on-line focusing in high-energy accelerators have limited focusing strengths (a few hundred MG/cm), while plasma lenses are able to produce focusing strengths a few orders of magnitude higher, depending on the plasma density. A plasma-lens, final-focus system might be even more important to achieve a reasonable luminosity in a proposed e^-e^- collider [2]. The self-focusing effect of a plasma on relativistic beams has been verified experimentally at Argonne National Laboratory [3], at Tokyo University [4], and more recently at UCLA [5]. The issue of luminosity enhancement by a self-ionized plasma at the Stanford Linear Collider (SLC) has been studied numerically by particle-in-cell simulations, and an enhancement factor of $\sim$5 is possible at the SLC center-of-mass energy ($\sim$ 92 GeV) [6].

Although the self-focusing effect of a plasma lens has been demonstrated experimentally, its practicability as a final-focusing device in e^+e^- linear colliders has yet to be verified. To this end, plasma-lens experiments have been proposed at the Final Focus Test Beam at SLAC [7]. Most importantly, the implementation of a plasma lens near a particle detector in future e^+e^- linear colliders requires that the presence of the plasma will not introduce serious backgrounds in the detector as a consequence of beam-plasma interactions. This paper gives a detailed account of detector backgrounds from a plasma lens. In section 2, we identify various sources of backgrounds and discuss the elementary physical processes responsible for their production. In section 3, we evaluate the cross section and event rate of each background source, using NLC [8] as an example. In section 4, we consider the effect of the backgrounds on various parts of a hypothetical NLC detector such as the vertex detector, the drift chamber and the calorimeter. Section 5 summarizes our results, which indicate that the background yields are small so that the performance of the main components of the detector will not be affected.

2 Sources of Backgrounds

Background particles produced by a plasma lens are of three types, namely, electrons and/or positrons, hadrons, and photons. The particles originate from different elementary physical processes underlying the interactions of the incoming electron or positron beam with the plasma of the lens located near the interaction point. In this section, we outline all the processes responsible for the various sources of backgrounds [9]. Their cross sections and angular distributions are calculated in the next section. From these results, the number of background particles can be determined for certain machine parameters; using NLC as an example, the prospect of the application of plasma lenses with acceptable backgrounds in future linear colliders is examined in a subsequent section.

(a) Electrons

Electrons and positrons arise from the scattering of the e^+ or e^- beam with the electrons of the plasma. The processes for producing electrons and positrons are:

Bhabha scattering,

$$e^+e^- \to e^+e^-,$$

Møller scattering,

$$e^-e^- \to e^-e^-,$$

elastic scattering,

$$e\,p \to e\,p,$$

and inelastic scattering,

$$e\,p \to e\,X.$$

(b) Hadrons

The hadronic backgrounds come from the elastic and inelastic scattering of the e^+ or e^- beam, and also from the inelastic scattering of photons (from synchrotron radiation and bremsstrahlung), with the protons in the plasma. Hadrons are produced by

elastic scattering,

$$e\,p \to e\,p,$$

and inelastic scattering,

$$e\,p \to e\,X,$$

$$\gamma\,p \to X.$$

(c) Photons

Photon backgrounds from a plasma are produced by

Compton scattering,

$$e\gamma \to e\gamma.$$

Three mechanisms produce the incident photons: synchrotron radiation at the final-focus quadrupole, synchrotron radiation as a consequence of plasma focusing, and bremsstrahlung of the e^+ or e^- beam in the plasma. These photons are then scattered by plasma electrons into large angles. Note that all detectors at e^+e^- colliders have to cope with photon backgrounds generated by synchrotron radiation scattering off masks or similar structures, which is not considered here.

3 Cross Sections and Event Rates

The cross section of an electron or a photon scattered by the plasma for a particular process is calculated by integrating its angular distribution

$$\sigma = \int_{\theta_c}^{\pi-\theta_c} \frac{d\sigma}{d\Omega} d\Omega, \tag{1}$$

where θ_c is the angular cut for the scattered particles into the detector, which is taken to be 150 mrad in our calculations. The number of scattered particles N_s for a bunch train is then given by

$$N_s = n_b \mathcal{L} \sigma, \tag{2}$$

where n_b is the number of bunches in a bunch train, and $\mathcal{L}$ is the beam-plasma luminosity per bunch crossing, respectively. The beam-plasma luminosity is given by

$$\mathcal{L} = N n_P d, \tag{3}$$

where N is the number of particles in a bunch, n_P is the plasma density and d is the thickness of the plasma. For our calculations, we take the NLC beam energy to be $E_{beam} = 250$ GeV, and $N = 0.65 \times 10^{10}$. We choose the hydrogen plasma density $n_P = 10^{18}$ cm^{-3} and $d = 1$ mm. We estimate that a plasma lens with these parameters will increase the luminosity for e^+e^- collisions from its nominal value by a factor of ~ 5. The beam-plasma luminosity $\mathcal{L}$ is 6.5×10^{26} cm^{-2}. For a bunch train of $n_b = 90$ bunches, $n_b\mathcal{L} = 5.85 \times 10^{28}$ cm^{-2}.

While the energy of the electrons in the beam is monochromatic, the energy of the photons incident on the plasma lens is not. The photons originating from the final-focus quadrupole and the plasma focusing follow the synchrotron-radiation spectrum, while those from bremsstrahlung in the plasma follow the Weizsäcker-Williams spectrum. Thus the photon distribution can be written as

$$n_\gamma(y) = n^p_{SR}(y) + n^q_{SR}(y) + n_{Brem}(y), \tag{4}$$

where $y = E_\gamma/E_{beam}$ is the ratio of the photon energy to the beam energy, $n_\gamma(y)$ is the total photon spectrum, and $n^p_{SR}(y)$, $n^q_{SR}(y)$, and $n_{Brem}(y)$ are the contributions from plasma-lens focusing, quadrupole focusing, and bremsstrahlung respectively. The synchrotron radiation spectrum from a focusing system can be approximated by the following expression [10]:

$$n^i_{SR}(y) = \frac{1}{\pi}\Gamma(\frac{2}{3})(\frac{\alpha d_i}{\sqrt{3}\gamma\lambda_e})(3\Upsilon_i)^{2/3}y^{-2/3}, \qquad 0 \lesssim y \lesssim \Upsilon_i, \quad i = p, q. \tag{5}$$

Here λ_e is the electron-Compton wavelength, γ is E_{Beam}/m_ec^2, d_i is the length of the focusing element ($d_q = 1$ m for a quadrupole and $d_p = 1$ mm for a plasma lens), and $\Upsilon_i = 2E^i_c/3E_{beam}$, where E^i_c is the synchrotron-radiation critical energy. For $y > \Upsilon_i$,

the synchrotron-radiation power is exponentially small and is neglected here. For a final-focus quadrupole, $\Upsilon_q \sim 1 \times 10^{-5}$ and $E_c^q \sim 2.5$ MeV; for the plasma lens considered here, $\Upsilon_p \sim 0.1$ and $E_c^p \sim 25$ GeV.

The bremsstrahlung spectrum from beam electrons scattered in the plasma is given by the Weizsäcker-Williams spectrum [11]

$$n_{Brem}(y) = \frac{2\alpha}{\pi y}[ln2.246 + ln\frac{m_p}{m_e} - \frac{1}{2} - lny], \tag{6}$$

where m_p and m_e are the proton and electron masses, respectively. Then the angular distribution of the cross section for each Compton process, after taking the photon spectrum into account, is given by

$$\frac{d\sigma}{d\Omega} = \int_0^{y_0} \frac{d\sigma(e\gamma \to e\gamma)}{d\Omega} n(y)dy, \tag{7}$$

where $n(y)$ is either the synchrotron radiation or the bremsstrahlung spectrum, and y_0 is the value above which radiation can be neglected, which is $\sim 1.5 \times 10^{-5}$, 0.15 and 1 for quadrupole focusing, plasma focusing, and bremsstrahlung in the plasma, respectively.

The integrated cross sections and backgrounds from the different processes are summarized in Table 1. We now discuss in more detail the production of each type of background particle.

(a) Electrons

The number of particles scattered into the detector depends on the angular acceptance, which is taken to be 150 mrad to $\pi - 150$ mrad from the incident-beam direction. When a 250-GeV electron or positron hits an electron at rest, the scattered particles go in the forward direction within a cone of very small opening angle about the direction of the incoming electron. Thus we expect a very small number of electrons scattered into the detector when a beam passes through the plasma lens. Electron backgrounds are essentially zero for Bhabha and Møller scatterings, since the scattered particles come out within the cone specified by our angular cut.

The angular distributions of the cross sections of the electrons and protons produced by elastic *ep* scattering are shown in Fig. 1. The cross section for electron production peaks highly in the forward direction. The total cross section for the imposed angular cut is 0.103×10^{-45} cm^{-2}, and hence, the contribution to the electron sources is negligibly small.

The angular distribution for the scattered electrons for inelastic *ep* scattering can be obtained by integrating the following differential distribution [12] over energy:

$$\frac{d\sigma}{dE'd\Omega} = \frac{\alpha^2}{4E^2\sin^4\frac{\theta}{2}}\{W_2(\nu, q^2)\cos^2\frac{\theta}{2} + 2W_1(\nu, q^2)\sin^2\frac{\theta}{2}\}. \tag{8}$$

Here E and E' are the incoming and outgoing electron energies respectively, $\nu = E - E'$, q^2 is the momentum transfer squared, and α is the fine-structure constant. The parametrizations of the structure functions $W_1(\nu, q^2)$ and $W_2(\nu, q^2)$ are taken from Ref. [13]. The

angular distribution of the cross section for inelastic *ep* scattering is shown in Fig. 2(a). Again, we see that the cross section peaks highly in the forward direction. The total cross section is 0.132×10^{-33} cm^2, which gives 0.8×10^{-6} electrons for a bunch train. Hence it can be concluded that the electron backgrounds due to the presence of a plasma lens can be neglected.

(b) Hadrons

While the electrons essentially move in the forward direction, the protons from *ep* elastic scattering are scattered into larger angles. In Fig. 1 we see that the differential cross section is a few orders of magnitude bigger than that for the electrons. Nevertheless, the integrated cross section is 0.613×10^{-39} cm^2 and hence the contribution to the proton sources is negligibly small.

For inelastic *ep* scattering, the initial-state proton can disintegrate into other particles; to properly take this effect into account we use HERWIG [14] to simulate the inelastic *ep* reactions of 250-GeV electrons with protons at rest. The differential distribution of charged hadrons as a function of scattering angle is shown in Fig. 2(b); it again peaks at small angles. The total cross section for the angular cut of 150 mrad is found to be 0.396×10^{-29} cm^2, which corresponds to about 0.23 charged hadrons for a bunch train at NLC energy. Thus, we expect the hadronic backgrounds from *ep* scattering will not pose problems to any component of a NLC detector.

For inelastic γp scattering, where the photon originates from one of the mechanisms mentioned in a previous section, we found from HERWIG simulations that the cross section does not vary sensitively with the incoming photon energy. Hence, we considered a monochromatic photon of 10 GeV interacting with a proton at rest for estimating the cross section. The integrated cross section is found to be 0.372×10^{-28} cm^2, which is about 8 times larger than that of the *ep* inelastic scattering. This corresponds to 2.2 charged hadrons for a bunch train, and hence the background is still very small.

(c) Photons

The photon backgrounds for the Compton process from the three photon sources depend on the photon spectrum. When the photon energy is much greater than the electron rest mass, the Compton cross section has a peak in the forward direction. When the photon energy is comparable to or less than the electron mass, the scattering is reduced to Thomson scattering and the angular dependence of the cross section varies as a dipole distribution. The angular distributions of the cross sections of the Compton process from the three photon sources are shown in Fig. 3. The bremsstrahlung spectrum is very soft; the angular distribution of this process is quite flat: it looks like a dipole distribution. The typical energy on the photon for synchrotron radiation from final quadrupole focusing is still small (on the order of one MeV) and hence, the distribution does not vary drastically with angle although it peaks moderately in the forward direction. Plasma focusing is much stronger than quadrupole focusing and the photon spectrum is expected to be harder with the typical energy of the order of 10 GeV. The cross section peaks in the forward direction and then drops rapidly at large angles. The total number of photons of all energies for a bunch train is $\sim$ 16,000, or about 180 for a single beam crossing. The

photon backgrounds from γp inelastic scattering are in general a few orders of magnitude smaller than those from Compton scattering, and hence can be neglected.

4 Detector Backgrounds

As discussed in Section 3, the leptons and hadrons scattered into the fiducial volume of a detector can be neglected.

The photons created by the different mechanisms calculated above cover a wide range of energy. Different components of future linear collider detectors are sensitive to certain energy windows of the energy spectrum of the outcoming photons. We now consider the photon backgrounds in a vertex detector, a drift chamber or TPC, and a calorimeter of an idealized NLC detector.

(a) Vertex detector

A brief description of the general characteristics of a pixel-based vertex detector for the NLC can be found in Ref. [15].

A minimum-ionizing charged particle will deposit 7.75 keV and generate about 2,100 electron-hole pairs in the, say, 20-μm-thick active Silicon of a vertex detector. Photons above 50 keV, for example, are unlikely to convert in the very thin structure of a barrel-vertex detector, which is expected to have a thickness of as little as 0.11% of a radiation length[15]. Thus, to be conservative, background photons of energies between, say, 4 keV and 100 keV need to be considered here. With these energy cuts, the number of background photons for the vertex detector is 3,600 for a bunch train, or only 40 per single-beam crossing, compared with 16,000 photons per bunch train at all energies. Even if one lowers the lower-energy cut to 1 keV (280 electron-hole pairs), close to the noise limit of about 250 pairs, the number of relevant photons increases only to about 50 per single-beam crossing or 4,500 per bunch train.

The angular distributions of the cross sections from different mechanisms are shown in Fig. 3 and they are dominated by Thomson scattering because of the relatively small energies. The cross section from bremsstrahlung photons is reduced almost by an order of magnitude because of the cut at the lower end of the soft Weizsäcker-Williams spectrum. The cross sections from quadrupole and plasma focusing photons are roughly reduced by a factor of 3.

For a vertex-detector barrel with a radius of 2.5 cm and with a length of 33 cm covering angles greater than 150 mrad ($|\cos\theta| \leq 0.99$), the density of photon tracks per unit surface area is $\sim 0.07/\mathrm{mm}^2$ for a bunch train, which is only about 7% of the acceptable occupancy of $\sim 1/\mathrm{mm}^2$. Even at the noise limit (1 keV lower cut), the occupancy remains below 10% of the value considered acceptable. Note that the choice of $|\cos\theta| \leq 0.99$ for the vertex detector is very generous. The number of background photons will be further reduced if the angular coverage is limited to, for example, $|\cos\theta| \leq 0.90$.

(b) Drift chamber

The next layer in the detector may well be a large drift chamber or TPC with about 10,000 sense wires. Such a drift chamber can easily tolerate 100 random background hits (1% occupancy). Assuming a 1% conversion probability, this allows for 10,000 incident photons. Photons of very small energies, say $\lesssim$10 keV, will be absorbed by the beam pipe and can be ignored. The conversion products of photons of less than, say 100 keV, will not form track segments. In a typical magnetic field they will form tight loops and deposit their energy locally. Proper design of the readout should account not only for the charge distribution typical of minimum-ionizing particles, but also for the sometimes large local depositions of energy from converting photons. Thus we need only to consider photons of energy greater than 100 keV scattered into the drift chamber.

The angular distributions of the cross sections above 100 keV are shown in Fig. 3. They all peak in the forward direction as a result of the hard-photon spectra from all the mechanisms. The total number of background photons with energy above 100 keV and scattering angle greater than 150 mrad is about 4,700 per bunch train, which is less than half of the acceptable number.

(b) Calorimeter

As mentioned above, leptons and hadrons will not be scattered into the main part of a detector in sufficient numbers to cause a problem for the calorimeter of a hypothetical NLC detector. Photons of very low energies will have been absorbed by the beampipe, drift-chamber walls, and similar structures before reaching the calorimeter. A typical calorimeter can possibly see energies as low as a few MeV; however, for any actual analysis, a cut is made removing clusters in a calorimeter with a total energy below, say, 100 MeV. Our simulation shows that of the total flux per bunch train of about 16,000 photons of all energies in the angular region with $|\cos\theta| \leq 0.99$, none have an energy above 100 MeV, and about 1,240 per bunch train, or $\sim$ 14 per single-beam crossing, have an energy between 1 and 100 MeV. While some of the latter might be seen in the innermost layer of electromagnetic calorimetry, they do not present a problem and are easily removed by a cluster cut, if isolated. The energy added by them to a shower created by a high-energy particle or jet is negligible compared to the intrinsic resolution of a typical calorimeter.

5 Summary

We summarize our background calculations in Table 1, which shows the various cross sections and particle fluxes for a single bunch crossing from the different background sources. As mentioned earlier, we have taken the NLC parameters as a reference. We have further assumed that the resolution time for the detector is much longer than 1.4 ns, the separation between successive bunches in a bunch train, but less than the $\sim$ 5 ms separation between bunch trains. Therefore, to be conservative, we integrated in our discussion the events over a train of 90 bunches for a total time span of $\sim$125 ns.

We have estimated only the sources of backgrounds from a plasma lens for a generic particle detector of a highly idealized machine but did not consider here the additional

sources of backgrounds that are common to any NLC detector, such as those due to beam scrapings or synchrotron radiation scattering off masks or similar structures. The discussion in Section 4 and Table 1 show that all the main components of the detector should survive the plasma-lens induced backgrounds. Thus the implementation of a plasma lens for luminosity enhancement in high-energy e^+e^- collisions is feasible without hampering the normal performance of the detector. Nevertheless, taking the present calculations as input, a more detailed and reliable estimate of the detector response to these background particles should be carried out by a *bona fide* detector simulation.

Acknowledgements

We thank T. Barklow, C.J.S. Damerell, S. Hertzbach, T. Markiewicz, S. Rajagopalan, D. Su, and E. Vella for useful discussions.

References

[1] P. Chen, *Part. Accel.* **17**, 121 (1987).

[2] C. A. Heusch, *The Case for e^-e^- Linear Colliders at High Energy*, Workshop on Physics and Experiments with Linear Colliders, F. A. Harris, S. L. Olsen, S. Pakvasa and X. Tata, ed., World Scientific (1993), p895.

[3] J. B. Rosenzweig *et al.*, *Phys. Fluids* **B2**, 1376 (1990).

[4] H. Nakanishi *et al.*, *Phys. Rev. Lett.* **66**, 1870 (1990).

[5] G. Hairapetian *et al.*, *Phys. Rev. Lett.* **72**, 2403 (1994).

[6] P. Chen, C.-K. Ng and S. Rajagopalan, *Phys. Rev.* **E48**, 3022 (1993).

[7] P. Kwok *et al.*, *Progress on Plasma Lens Experiments at the Final Focus Test Beam*, Proc. of Particle Accelerator Conference, Dallas, May 1-5, 1995, to be published.

[8] T.Raubenheimer *et al.*, *Parameters of the SLAC Next Linear Collider*, Proc. of Particle Accelerator Conference, Dallas, May 1-5, 1995, to be published.

[9] C. Baltay, *Backgrounds in SLD due to the Proposed SLC Plasma Lens*, SLD Internal Note, 1992, unpublished.

[10] P. Chen, *Beamstrahlung and the QED, QCD Backgrounds in Linear Colliders*, SLAC-PUB-5914, 1992; and in *Photon-Photon Collisions*, D. O. Caldwell and H. P. Paar, ed., World Scientific (1992).

[11] See, for example, J. D. Jackson, *Classical Electrodynamics*, 2nd ed. John Wiley & Sons (1975), p724.

[12] See, for example, F. Halzen and A. D. Martin, *Quarks and Leptons*, New York, Wiley (1984), p179.

[13] J. Kwiecinski, A. D. Martin, R. G. Roberts and W. J. Stirling, *Phys. Rev.* **D42**, 3645 (1990).

[14] G. Marchesini *et al.*, HERWIG: *A Monte Carlo Event Generator for Simulating Hadron Emission Reactions with Interfering Gluons*, *Comp. Phys. Comm.* **67**, 465 (1992).

[15] C. J. S. Damerell, *Vertex Detectors at Linear Colliders (Present and Future)*, RAL Report RAL-94-096, 1994.

Table:

Background source	Cross section (cm^{-2}) $\lvert\cos\theta\rvert \leq 0.99$	Vertex detector	Drift chamber
Bhabha and Møller e^+, e^-	0	0	0
Elastic ep: e	0.103×10^{-45}	negligible	negligible
p	0.613×10^{-39}	negligible	negligible
Inelastic ep: e	0.132×10^{-33}	negligible	negligible
charged hadrons	0.396×10^{-29}	0.003	0.003
Inelastic γp: charged hadrons	0.372×10^{-28}	0.02	0.02
Compton γ's from quadrupole	0.995×10^{-25}	23	29
Compton γ's from plasma focusing	0.548×10^{-25}	11	20
Compton γ's from bremsstrahlung	0.119×10^{-24}	6	3

Table 1: Summary of background sources from a plasma lens in NLC for a single beam crossing. Each bunch has 0.65×10^{10} particles; the plasma density is 10^{18} cm^{-2}, length 1 mm. The cross sections are integrated as in Eqs. (1), (7); see Section 4 for additional energy cuts imposed in the calculation of particle numbers in the last two columns.

Figure Captions:

Fig. 1. Angular distributions of the cross sections in the laboratory frame for ep elastic scattering. The energy of the incoming electron is 250 GeV and the proton is at rest.

Fig. 2. (a) Angular distribution of the cross section in the laboratory frame for the scattered electrons for ep inelastic scattering.
(b) HERWIG angular distribution of charged hadrons for 20,000 events for ep inelastic scattering. The total cross section is normalized to 1.02×10^7 pb.

Fig. 3. Angular distributions of the Compton cross sections from various sources of photons: bremsstrahlung in plasma, quadrupole focusing, and plasma-lens focusing. The solid lines are for the whole energy range, the dashed lines for the energy range between 4 keV and 100 keV (relevant for the vertex detector), and the dotted lines for energy greater than 100 keV (relevant for the drift chamber).

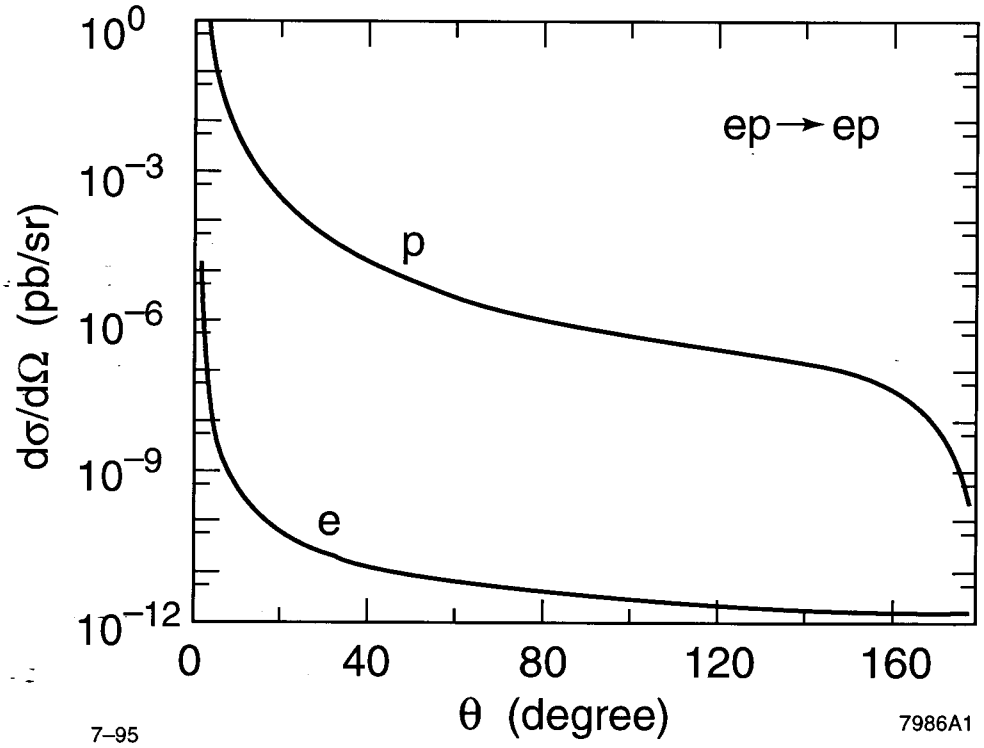
10^0
10^{-3}
10^{-6}
10^{-9}
10^{-12}
$d\sigma/d\Omega$ (pb/sr)
ep → ep
p
e
0
40
80
120
160
θ (degree)
7–95
7986A1

Fig. 1

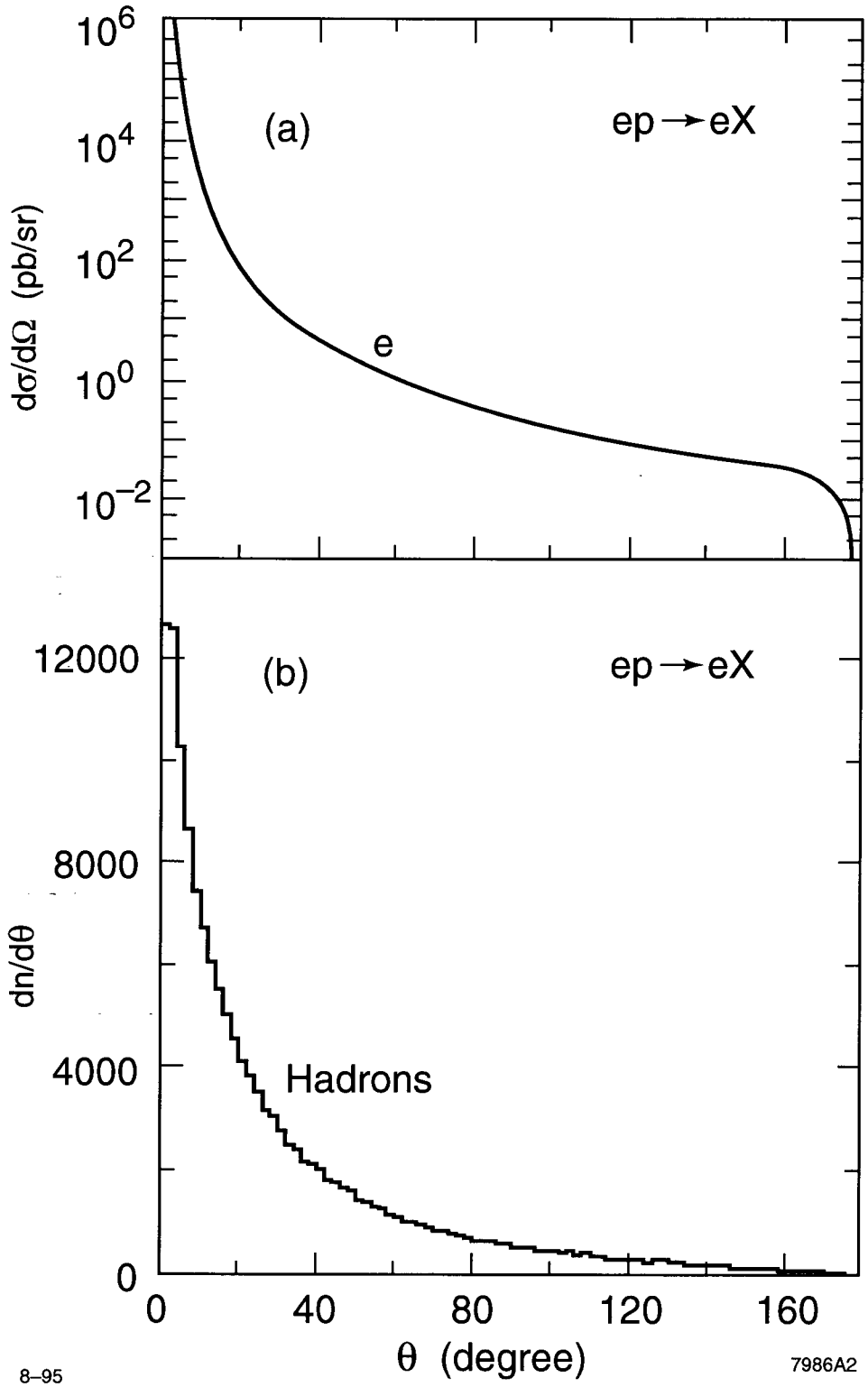
(a)
ep → eX
e
dσ/dΩ (pb/sr)
10^6
10^4
10^2
10^0
10^{-2}
(b)
ep → eX
Hadrons
dn/dθ
12000
8000
4000
0
0
40
80
120
160
θ (degree)
8–95
7986A2

Fig. 2

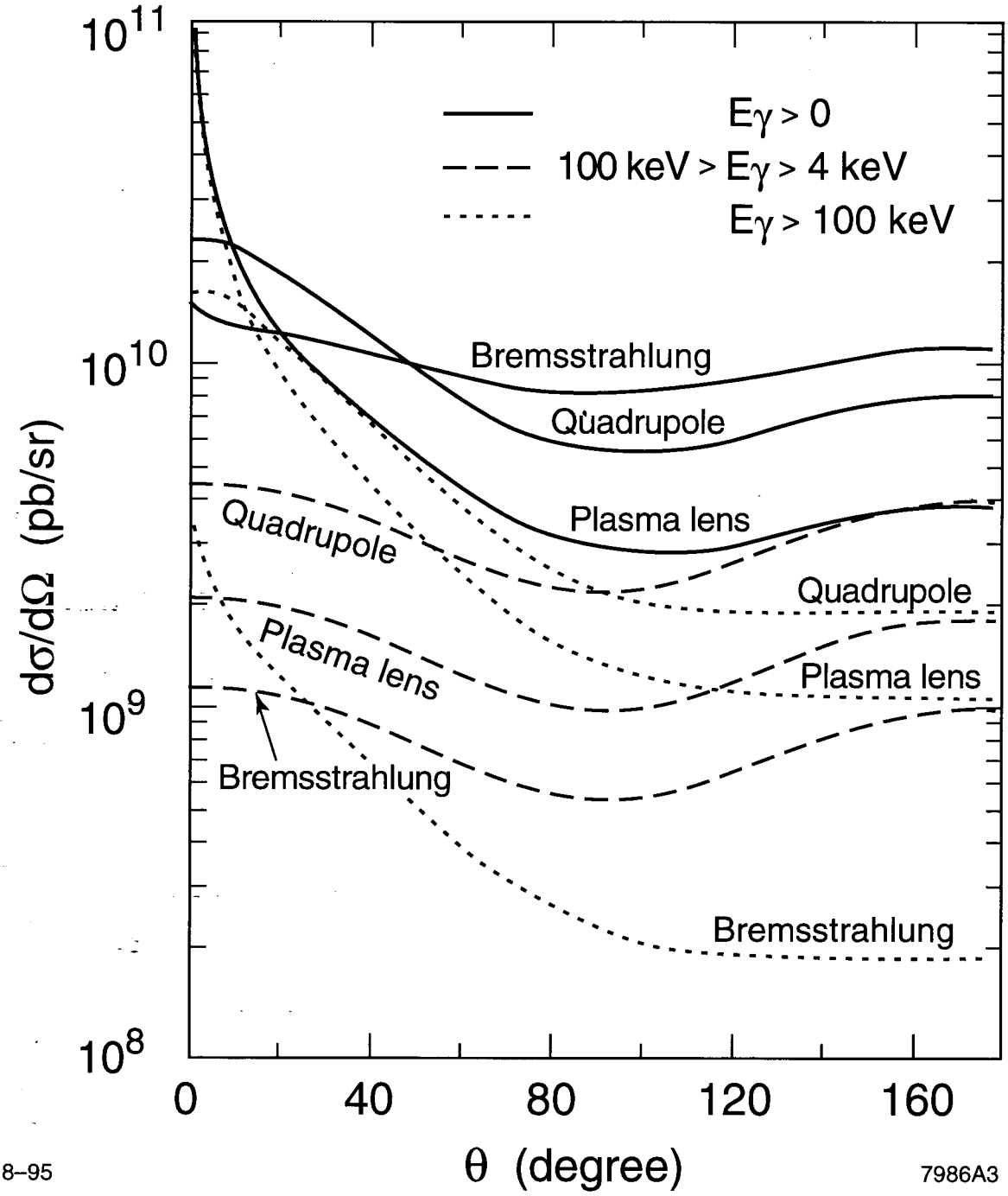
10^{11}
10^{10}
10^{9}
10^{8}
$d\sigma/d\Omega$ (pb/sr)
$E\gamma > 0$
100 keV > $E\gamma$ > 4 keV
$E\gamma$ > 100 keV
Bremsstrahlung
Quadrupole
Plasma lens
Quadrupole
Plasma lens
Quadrupole
Plasma lens
Bremsstrahlung
Bremsstrahlung
0
40
80
120
160
θ (degree)
8–95
7986A3

Fig. 3